K-shell photoabsorption spectrum of C II

E. Jannitti
Istituto Gas Ionizzati, Consiglio Nazionale delle Ricerche, Via Gradenigo 6/A, 35131 Padova, Italy

M. Gaye
Dipartimento di Elettronica e Informatica, Via Gradenigo 6/A, 35131 Padova, Italy

M. Mazzoni
Dipartimento di Astronomia, Largo Enrico Fermi 5, 50125 Firenze, Italy

P. Nicolosi and P. Villoresi
Dipartimento di Elettronica e Informatica, Via Gradenigo 6/A, 35131 Padova, Italy
(Received 6 April 1992; revised manuscript received 16 November 1992)

The K-shell photoabsorption spectrum of C II has been obtained with a technique using two laser-produced plasmas. Both the discrete spectrum as well as the photoionization continuum have been observed. Precise wavelength measurements and atomic structure calculations have been performed. The discrete lines have been identified and correspond to transitions of the 1s inner electron starting from the ground or low excited levels. The $1s^22s^22p$-$1s2s^22pnp$ series has been observed up to $n=6$. The limits were estimated as 2 549 000 cm^{-1} (316.0 eV) and 2 570 000 cm^{-1} (318.6 eV) and checked against the corresponding C III levels. The relative photoionization cross section from the threshold, at about 318 eV, up to 500 eV, has also been measured.

PACS number(s): 32.30.Jc, 32.80.Fb

INTRODUCTION

Absorption spectroscopy is a very useful method for the analysis of the atomic, molecular, and solid-state structure and has been extensively applied to many neutral species. On the contrary, in spite of its importance, very little absorption spectroscopy of ionized species has been performed to date. The reason is mainly due to the difficulty in generating a suitably dense, stable, and reproducible absorbing column of multicharged ions, with a line density sufficient to allow reliable absorption measurements. Indeed, these conditions can be satisfied, only for a very short time, in laboratory experiments utilizing laser-produced plasmas. It is then possible to perform absorption measurements of ionized species, backlighting the absorbing plasma column with a pulsed and synchronized background continuum source of shorter time duration.

In the past we have extensively studied laser-produced plasmas (LPP's), through spectroscopic observations and diagnostics, and we have measured their main parameters, such as temperature and density, their spectral emission, and their physical characteristics, such as the spatial and the temporal dynamics [1–3]. In particular, it has been shown that the LPP can be utilized very advantageously as a pulsed continuum source as well. In fact, due to the high xuv conversion efficiency in the laser-matter interaction process, a strong and spectrally smooth continuum can be easily obtained in the xuv spectral range by focusing onto high-Z materials a laser pulse, even of only a few joules. The most relevant characteristics of this continuum source are the short time duration, comparable to that of the laser pulse, its small physical size, and its high brightness [4].

During the past few years we have implemented and, since the first experiments [5], improved the absorption technique of two LPP's, one acting as an absorbing ionized medium, the other as a background continuum source. The technique permits one to measure the absorption spectrum of a single ion, among the different ones produced in the absorbing plasma. For this purpose the following parameters must be optimized during the experiment: the time delay between the generation of the two plasmas; the backlighting distance, i.e., the distance from the target surface of the point wherein the background continuum pass through the expanding absorbing plasma; the laser power density used for generating the absorbing ionized medium. We have widely studied the absorption spectra of Be, B, and C ions both in grazing- and normal-incidence spectral regions, showing the high reliability of the technique. In particular, outer-shell and inner-shell measurements of both the discrete transitions and the photoionization cross sections have been performed [6–11]. Even if very few with respect to the whole of ion absorption spectra, our results represent the first effort of a systematic analysis, starting from low-Z ions, to our knowledge.

For a better understanding of the present experimental technique, it can be useful to point out briefly the features that make the LPP well suited as an absorbing medium of ionized species. First, there is no limit, in principle, for the maximum ionization stage to be produced. Indeed, it depends on the laser power density focused onto the target and, for instance, only a few joules of laser energy, in

15 ns, are typically enough to produce H-like ions from low-Z targets. Besides, the generated ions have different time evolution and density distribution, according also to the laser power density focused onto the absorbing target. The more highly ionized species, such as H-like or He-like ions of low-Z materials, have the highest expansion velocities and a time duration comparable to the laser-pulse width, while lower-charged ions show lower velocities and longer time durations. Therefore in the expanding plasma the more stripped ions are the first to appear and are followed in turn by ions of successively lower ionization. Practically, the lower-charged ions expand out from the target surface after the laser pulse is over and neutral atoms and vapors are emitted as well [11]. As regards the spatial distribution of the ion species throughout the expanding plasma, the ions with higher charge expand symmetrically concentrated in a small solid angle around the normal to the target, while the lower-charged ones have a wider spread [12]. In conclusion, in the expanding plasma the individual ion species tend to be separated in space and in time more and more with distance from the target surface.

Such characteristics show that the two LPP absorption techniques can be well suited to obtain the absorption spectrum of an individual ion species, in the whole of the different ones produced in the absorbing plasma. In fact, it appears sufficient to generate the plasma emitting the background continuum with a proper time delay after the absorbing plasma. Clearly this time delay must be correlated to the laser power density used for generating the absorbing plasma and to the distance from the target more convenient for the backlighting. As concerns the latter, it must be taken into account that the best spatial resolution usually is obtained backlighting the absorbing plasma, with the delayed continuum, at as great as possible distance from the target surface. Obviously there is a limit to the maximum useful distance that can be used in the experiment, because, due to the expansion, the value of line density of the absorbing plasma decreases with the distance from the target, while it must be kept high enough to perform reliable absorption measurements. For instance, a low value of line density tends to lower the signal-to-noise (S/N) ratio in the measurements. The S/N ratio, however, can be increased, performing and accumulating many measurements for each spectrum, and this can be done only if the generated plasmas are reproducible. The LPP shows very high pulse by pulse reproducibility, ensuring good statistics in the experimental results.

Even if the application of this technique seems very simple, indeed some technical difficulties can partially invalidate its effectiveness in resolving the absorption spectrum of a single ion. The difficulties increase, especially when absorbing ionized materials with higher atomic number Z are analyzed, because the spatial and temporal separation of the different ions that expand out from the target surface becomes smaller. In the following, the main parameters that can affect the results of the experiment are briefly described.

Firstly, in order to have the best spatial resolution, it is necessary to backlight the absorbing plasma in a spatial region as small as possible around the required distance from the target. The amplitude of this spatial region should be smaller than the separation of the different expanding ions and this is difficult to achieve in the grazing-incidence spectral region. In our experiment we have been able to get a high spatial resolution, collecting and focusing the background continuum with a toroidal mirror, working at grazing incidence. Besides, in order to achieve good time resolution, the time duration of the background continuum must be as short as possible, especially if highly charged short-lived ions have to be analyzed. Also in this case it can be convenient to increase the backlighting distance, because, due to the spread in the expansion velocity, the time duration of each ion species increases with the distance from the target. On the contrary, low charged ions have a time duration longer than the background continuum and can be probed at small distances from the target surface as well.

Finally, a very important effect can occur in the generation of the absorbing plasma, if the laser power density through the focal spot focused on the target is not uniform. In fact, ions with different charges can be generated from separate points of the focal spot, and a nonuniform ion distribution is propagated in the expanding plasma. This phenomenon reduces the possibility of resolution between different absorption spectra and becomes more marked when a line focusing or defocusing technique is used for increasing the line density of the absorbing plasma, particularly if high-Z materials are used. Only a suitable apodization of the radial energy distribution in the laser beam can reduce this effect. Otherwise it can be strongly reduced by focusing the laser beam to a very small focal spot, as can be done when highly charged ions must be produced.

In this paper we report the C II K-shell absorption spectrum in the range 25–45 Å. As it has been previously obtained for Be, we have now completed the K-shell isonuclear sequence of C in the xuv. In particular, the latter ranges from the solid C film and vapor spectra up to the He-like C V spectrum [13]. The present spectrum has been obtained through a careful optimization of the various experimental parameters, for minimizing the contribution due to other ionization stages. Both the discrete part of the spectrum and the photoionization continuum have been observed. Accurate wavelength measurements as well as Hartree-Fock calculations of the observed discrete transitions have been performed. The discrete lines have been identified and correspond to transitions of the 1s inner-shell electron, starting from the ground or low excited levels. The $1s^22s^22p$-$1s2s^22pnp$ series up to $n=6$ has been observed. The limits were estimated as 316.0 and 318.6 eV and checked against the corresponding C III levels. The relative photoionization cross section has also been measured from the threshold, at about 318 eV, up to 500 eV and it appears to be consistent with the theoretical prediction of Reilman and Manson [14].

EXPERIMENT

The experimental setup has been widely described elsewhere [8,15], to which the reader is referred to for more

details. A block scheme of the experiment is, however, reported in Fig. 1. Practically two plasmas are generated, with a suitable time delay, by focusing two laser beams on plane solid targets. A Q-switched ruby laser beam of about 7 J of energy and 15-ns duration is split into two beams. One beam, with about 70% of the total laser energy, is optically delayed and then is sharply focused onto a tungsten (W) target with an aspheric lens; the resulting focal spot diameter is about 30 μm. The generated plasma emits a pulse, lasting about 20 ns, of strong and smooth xuv continuous radiation, used as background continuum in the experiment. This continuum is collected by a toroidal mirror, working at grazing incidence ($\sim 87°$), and, suitably utilizing its astigmatism, is focused first onto the entrance slit of the spectrograph and then to a diffracted wavelength position on the focal surface. The toroidal mirror looks directly at the ablation region of the W plasma, where the electron density reaches its maximum value. Note that the continuum emission is mainly due to the recombination and bremsstrahlung processes, whose intensities depend on the electron density. The spectrograph is equipped with a 1200-l/mm, 2-m radius, spherical grating working at 86° angle of incidence, in the classical Rowland scheme. The toroidal mirror compensates the astigmatism of the grating considerably and, acting as a light condenser, fills the aperture of the spectrograph. The latter is very important for keeping as high as possible the S/N ratio of the measurements.

The absorbing carbon plasma has been produced by focusing the second laser beam with a spherocylindrical lens onto a graphite target; in this way the length of the absorbing column and, consequently, the measured absorption coefficient are increased. Besides, the focal spot size and the energy of the laser beam have been optimized, in order to give the expected ionization degree of the plasma. The resulting spot size was (0.2×10) mm^2, corresponding to about 3.5 GW/cm^2 of power density.

The absorbing plasma is generated close to the entrance slit of the spectrograph. In this way only a small region (~ 0.2 mm) of the plasma is probed by the background continuum. The distance from the target can be varied by moving the C target up and down. The C absorbing plasma has been probed at 0.5 mm from the target and the W plasma has been generated after a delay of 55 ns.

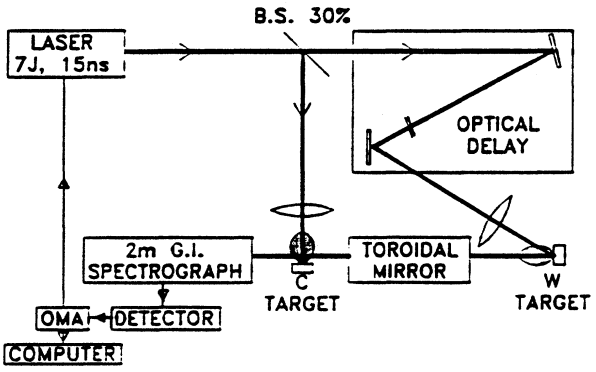

FIG. 1. Scheme of the experiment including a beam splitter (BS), an optical multichannel analyzer (OMA), and a grazing-incidence (GI) spectrograph.

The detection system consists of a 10–20-μm-thick scintillator coating, deposited on a plane fiber-optic faceplate. Television-type phosphors (Kyokko P45), with a grain average size of about 3 μm, have been used and deposited with a standard technique. The faceplate is coupled to a linear photodiode array via a coherent flexible bundle and is movable with a trolley along the Rowland cylinder. The scintillator coating provides the conversion of the xuv radiation into visible light, which is transmitted coherently to the photodiode array. The latter has 512 elements (pixels) with 25 μm of spatial width, corresponding to 0.012 Å/pixel on the Rowland cylinder. The signal is finally processed with an optical multichannel analyzer (OMA) and a personal computer (PC). The advantages of this detection system, with respect to the photographic technique, are the good linearity, the large dynamic range, and the real-time data examination.

Essentially in a standard acquisition procedure the background continuum $I_0(\lambda)$, the absorption spectrum $I(\lambda)$, and, when detectable, the emission spectrum from the absorbing plasma $I_e(\lambda)$ are recorded in succession and the absorption coefficient $K(\lambda)$ is derived according to the relation

$$K(\lambda)=\ln\frac{I_0(\lambda)}{I(\lambda)-I_e(\lambda)} . \tag{1}$$

The statistical accuracy as well as the S/N ratio of the measurements have been obviously greatly improved by averaging over several acquisitions. In this respect, as already mentioned, the two LPP's have been checked shot by shot and indeed they proved very reproducible. The wavelength calibration has been performed by recording some reference lines on the absorption spectra. Emission lines from Al and brass (Zn and Cu) plasmas and some well-identified and independently measured C absorption lines have also been used as standards. During the registration of the reference spectra, the Al and brass targets must be placed in the same position of the W target, within a few micrometers, in order to avoid any relative sagittal displacement between the reference and the absorption spectrum in the spectrograph focal surface. In fact, the recorded spectra are nearly stigmatic in this surface, because the toroidal mirror provides a sagittal focalization, which compensates the astigmatism of the spherical grating. Accordingly, if the reference and W targets are positioned in different points in the front focal plane of the toroidal mirror, the position and the dispersion of the two spectra, in the focal surface, are different and this invalidates the wavelength calibration. In addition, each exposure, corresponding to 10–30 acquisitions, has been taken within 3–4 h, interposing the acquisition of the standards at regular time intervals. In this way the effect of possible thermal stresses of the experimental equipment has been considerably reduced. Finally, the nonuniform response of the scintillator coating has been taken into account. While it does not affect the absorption

coefficient, which is derived from the ratio between the absorption and the continuum spectra, it can deeply affect the emission spectra. In fact, possible small irregularities of the scintillator layer, enhanced by the grazing incidence, can produce a local different conversion efficiency. This can give some distortion of the observed line profiles, appearing as a pseudo spectral shift. For this reason the reference emission spectra have been corrected for the flat-field response of the scintillator.

C II ABSORPTION SPECTRUM

The experimental measurement of the K-shell absorption coefficient of C II is reported in Fig. 2. The values of the various experimental parameters, such as laser power density, delay, etc., have already been mentioned. This spectrum has been obtained joining four adjacent, partially overlapping spectral regions, because of the limited length of the photodiode array (512 pixels), corresponding to about 6.4 Å in the spectrograph focal surface. It clearly shows the series of discrete lines converging to the photoabsorption threshold at about 39 Å and the photoionization continuum down to 25 Å. The latter exhibits a good agreement with the cross section computed by Reilman and Manson [14] (dashed curve), normalized at the threshold value, well within the uncertainty of the computed values.

Any contribution due to the emission of the absorbing plasma and to the stray light by the background continuum was not measurable, simplifying the experiment; the latter, in particular, is not accounted for, like the emission, in the formula used for the absorption coefficient and could decrease, if any, the peak value of the absorption coefficient. Besides, the measured absorption coefficient between discrete lines was very low, showing that contribution due to the scattering by the absorbing plasma is negligible. In fact, it should give a background absorption, practically independent of the wavelength.

The discrete portion of the spectrum has been deconvoluted for deriving the real absorption coefficient of the lines. In fact, the spectral line shapes are strongly affected by the finite instrumental resolving power. For this reason the instrumental function of the system has been carefully measured and fitted with a Voigt profile with a full width at half maximum (FWHM) of about 0.05 Å. Then a constrained deconvolution procedure has been applied to the absorptance. The latter is defined as

$$A(\lambda)=1-\frac{I(\lambda)}{I_0(\lambda)} \tag{2}$$

and is constrained between 0 and 1 in an iterative deconvolution process as described in [16].

The contributions of the adjacent atomic species C III and C I are very weak and do not affect the photoionization continuum of C II. Practically only the strongest lines of these ions are present and can be easily identified. In fact, for a small variation of the experimental parameters, e.g., the delay or the backlighting distance from the carbon target, the absorption coefficient of the C II varies very little, while that of the adjacent ions becomes manifestly stronger for the ion more favored by the new experimental conditions, and weaker for the other. This effect appears very helpful in selecting the requested ionization stage.

The discrete part of the C II spectrum has also been studied in more detail using a tapered faceplate to increase the resolving power of the detection system by a factor of 2. In this way the equivalent pixel size on the focal surface results about 12.5 μm along the spectral direction, corresponding to about 0.006 Å/pixel. While it does not affect the spectral resolution of the spectrograph, this solution allows one to obtain a higher frequency sampling through the line profiles, and this reduces the uncertainty in the best-fit process and improves the determination of the shape and position.

Figures 3(a) and 4(a) show the expanded portion of the spectra centered, respectively, around 43.0 and 40.3 Å, and obtained with the tapered faceplate, while in Figs. 3(b) and 4(b) the same spectra, resulting after the constrained deconvolution process, are reported. It appears noteworthy that several lines have been resolved from the observed blended features, considerably improving the final resolution. Obviously the fidelity of the deconvolution process is strongly dependent on the S/N ratio and on the width of the spectral lines with respect to the width of the instrumental profile. The latter exhibits a FWHM of about 0.03 Å and affects, above all, the peak value of the resulting absorption coefficient of the discrete lines. The spectra shown in Figs. 3 and 4 have been recorded in slightly different conditions with respect to the spectrum reported in Fig. 2. Essentially here care has been taken mostly on the discrete portion of the C II spectrum. For this reason these spectra have been obtained by probing the carbon plasma with the back-

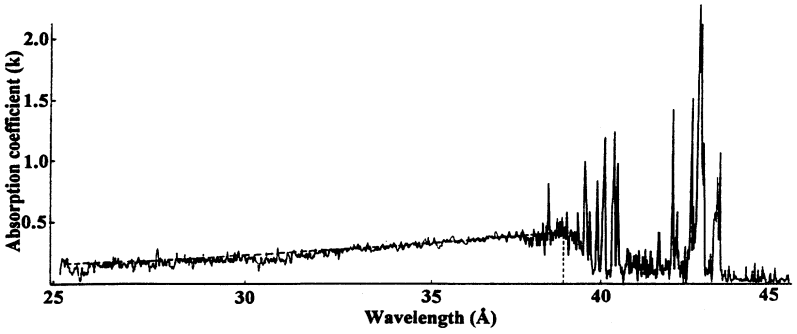

FIG. 2. C II absorption-coefficient spectrum.

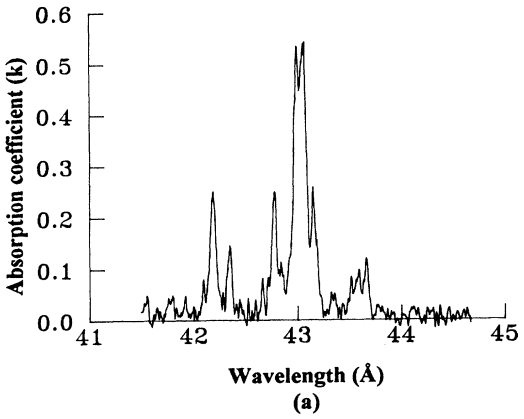

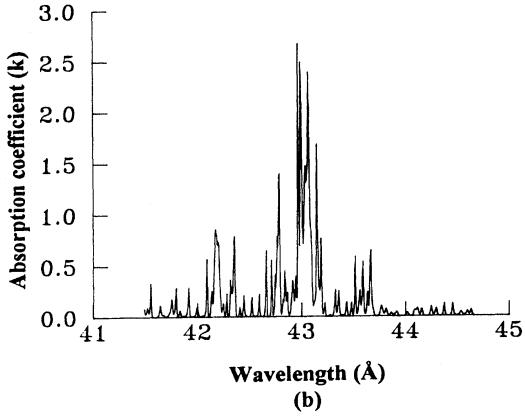

FIG. 3. Spectrally expanded portion of the C II absorption coefficient (a) before and (b) after the constrained deconvolution process.

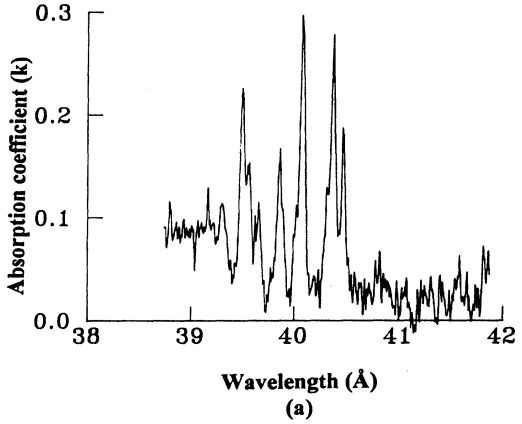

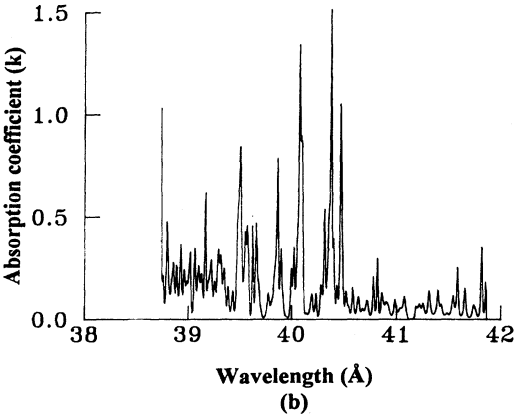

FIG. 4. Spectrally expanded portion of the C II absorption coefficient (a) before and (b) after the constrained deconvolution process.

ground continuum at 1 mm from the C target and with a delay of 80 ns between the two plasmas.

SPECTRUM OF THE 1*s* INNER ELECTRON

Careful wavelength measurements have been performed by fitting the superimposed standards with the dispersion curve of the grating. An analytical correction has been applied to the fitting process to take into account that the plane faceplate does not exactly match the Rowland cylinder. The averaged wavelength measurements, together with the corresponding absorption coefficient, are reported in Table I. The estimated accuracy is, for most of the lines, within ± 0.01 Å. The absorption coefficient is greatly affected by uncertainties in the deconvolution process. Almost all the detected peaks can be accounted for as transitions giving rise to single core-excited states, namely, as jumps of a *K*-shell electron. In most cases, these transitions occur while one or more excited electrons of the *L* shell are present as a spectator. On the whole, the spectroscopic features of C II are a main extended series starting from the lowest ground state, along with transitions arising from several different configurations, when one or more of the outer electrons are excited; these features are similar to the ones we have already identified in the absorption spectra by light ions (Be, B), obtained with the same technique [8,9,17]. But, unlike other examined spectra, here there are more possible low-lying initial configurations and the five electrons of C II originate a considerable number of lines, all included in a range of a few Å. The present knowledge of the core-excited structure of C II is rather poor. Some inner-shell transitions have already been observed and tentatively identified in a work on Auger spectra by Rødbro, Bruch and Bisgaard [18], who also reported previous calculations and measurements; however, their assignments only dealt with levels of the $1s2s^22p^2$ configuration.

This investigation has been accomplished with the help of Hartree-Fock (HF) computations, including relativistic corrections; it has been carried out by means of the Cowan program suite [19] as far as the core-excited levels

TABLE I. C II inner-shell transitions.

λ_{expt} (Å)	K	Configurations	λ_{calc} (Å)
43.651		C I	
43.581		C I	
43.506		C I	
43.180	0.8	$1s^2 2p^3\,^2P - 1s(2p^4\,^1D)^2D$	43.191
		$1s^2 2s 2p^2\,^4P - (1s2s\,^1S)(2p^3\,^4S)^4S$	43.186
		$1s^2 2p^3\,^2P - 1s(2p^4\,^3P)^2P$	43.172
43.146	1.7	$1s^2 2p^3\,^4S - 1s(2p^4\,^3P)^4P$	43.146
43.115	1.2	$1s^2 2s 2p^2\,^2S - (1s2s\,^1S)(2p^3\,^2P)^2P$	43.112
43.064	2.4	$1s^2 2s^2 2p\,^2P - 1s2s^2(2p^2\,^1D)^2D$	43.064
43.033	1.5	$1s^2 2s 2p^2\,^4P - (1s2s\,^3S)(2p^3\,^2D)^4D$	43.047
42.997	1.9	$1s^2 2s 2p^2\,^2P - (1s2s\,^3S)(2p^3\,^2D)^2D$	43.000
42.983	1.0	$1s^2 2s 2p^2\,^2D - (1s2s\,^1S)(2p^3\,^2D)^2D$	42.980
42.962	2.1	$1s^2 2s^2 2p\,^2P - 1s2s^2(2p^2\,^3P)^2P$	42.962
42.913	0.6		
42.853	0.4	$1s^2 2p^3\,^2D - 1s(2p^4\,^1D)^2D$	43.852
42.834	0.6	$1s^2 2p^3\,^2D - 1s(2p^4\,^3P)^2P$	42.834
42.801	0.7		
42.782	1.5	$1s^2 2s 2p^2\,^4P - (1s2s\,^3S)(2p^3\,^2P)^4P$	42.782
42.761	0.8	$1s^2 2s 2p^2\,^2P - (1s2s\,^3S)(2p^3\,^4S)^2S$	42.761
		$1s^2 2p^3\,^2P - 1s(2p^4\,^1S)^2S$	42.750
42.741	0.6	$1s^2 2s^2 3p\,^2P - 1s2s^2 2p(^3P)3p\,^2P$	42.739
		$1s^2 2s 2p^2\,^2P - (1s2s\,^3S)(2p^3\,^2P)^2P$	42.735
42.707	0.4	$1s^2 2s 2p^2\,^2D - (1s2s\,^1S)(2p^3\,^2P)^2P$	42.715
42.675	0.6	$1s^2 2s^2 2p\,^2P - 1s2s^2(2p^2\,^1S)^2S$	42.675
42.619	0.5	$1s^2 2s^2 3p\,^2P - 1s2s^2 2p(^3P)3p\,^2D$	42.632
42.347	0.8	$1s^2 2s 2p^2\,^2D - (1s2s\,^3S)(2p^3\,^2D)^2D$	42.350
42.315	0.4	$1s^2 2s^2 3s\,^2S - 1s2s^2 2p(^1P)3s\,^2P$	42.315
42.292	0.5	$1s^2 2s^2 3p\,^2P - 1s2s^2 2p(^1P)3p\,^2P$	42.300
42.205	0.8	$1s^2 2s^2 3d\,^2D - 1s2s^2 2p(^1P)3d\,^2D$	42.206
42.194	0.8	$1s^2 2s^2 3d\,^2D - 1s2s^2 2p(^1P)3d\,^2F$	42.191
42.175	0.8	$1s^2 2s^2 3d\,^2D - 1s2s^2 2p(^1P)3d\,^2P$	42.168
		$1s^2 2s 2p^2\,^4P - 1s2s(^3S)2p^2(^5P)3p\,^4D$	42.157
42.088	0.5	$1s^2 2s 2p^2\,^2D - (1s2s\,^3S)(2p^3\,^2P)^2P$	42.093
41.787	0.4	$1s^2 2s 2p^2\,^2D - 1s2s(^3S)2p^2(^3D)3p\,^2F$	41.796
40.805	0.5		
40.767	0.4		
40.460	0.9	$1s^2 2s^2 2p\,^2P - 1s2s^2 2p(^3P)3p\,^2P$	40.460
40.366	1.5	$1s^2 2s^2 2p\,^2P - 1s2s^2 2p(^3P)3p\,^2D$	40.366
40.303	0.5	$1s^2 2s^2 2p\,^2P - 1s2s^2 2p(^3P)3p^2\,^2S$	40.304
40.350	0.4		
40.331	0.1		
40.086	0.6	$1s^2 2s^2 2p\,^2P - 1s2s^2 2p(^1P)3p\,^2D$	40.087
40.068	1.2	$1s^2 2s^2 2p\,^2P - 1s2s^2 2p(^1P)3p\,^2P$	40.068
40.040	0.3	$1s^2 2s^2 2p\,^2P - 1s2s^2 2p(^1P)3p\,^2S$	40.033
39.891	0.2	$1s^2 2s^2 2p\,^2P - 1s2s^2 2p(^3P)4p\,^2P$	39.888
39.856	0.9	$1s^2 2s^2 2p\,^2P - 1s2s^2 2p(^3P)4p\,^2D$	39.858
		$1s^2 2s^2 2p\,^2P - 1s2s^2 2p(^3P)4p\,^2S$	39.836
39.649	0.5	$1s^2 2s^2 2p\,^2P - 1s2s^2 2p(^3P)5p\,^2P$	39.640
39.613	0.7	$1s^2 2s^2 2p\,^2P - 1s2s^2 2p(^3P)5p\,^2D$	39.623
		$1s^2 2s^2 2p\,^2P - 1s2s^2 2p(^3P)5p\,^2S$	39.612
39.560	0.4	$1s^2 2s^2 2p\,^2P - 1s2s^2 2p(^1P)4p\,^2D$	39.559
		$1s^2 2s^2 2p\,^2P - 1s2s^2 2p(^1P)4p\,^2P$	39.554
39.541	0.4	$1s^2 2s^2 2p\,^2P - 1s2s^2 2p(^1P)4p\,^2S$	39.544
39.500	0.5	$1s^2 2s^2 2p\,^2P - 1s2s^2 2p(^3P)6p\,^2P$	39.495
39.480	0.4	$1s^2 2s^2 2p\,^2P - 1s2s^2 2p(^3P)6p\,^2D$	39.486
		$1s^2 2s^2 2p\,^2P - 1s2s^2 2p(^3P)6p\,^2S$	39.480
39.280	0.3	$1s^2 2s^2 2p\,^2P - 1s2s^2 2p(^1P)5p\,^2P$	39.299
39.154	0.5	$1s^2 2s^2 2p\,^2P - 1s2s^2 2p(^1P)6p\,^2P$	39.159
38.784	0.4	C III	

are concerned, whereas the excited outer levels were taken from tables [20]. The analysis leads to the identification of the single-electron transitions, $1s$-np, occurring in the following configurations:

$$1s^2 2s^2 2p;\ 1s^2 2s 2p^2;\ 1s^2 2s^2 3s;\ 1s^2 2s^2 3p;\ 1s^2 2p^3;$$

$$1s^2 2s^2 3d\ .$$

The measured wavelengths, the experimental peaks absorption coefficients, the suggested assignments, and the corresponding theoretical values are reported in Table I. Unfortunately, some lines often lie so close to each other, compared with the present spectral resolution, that they strongly blend and a double assignment is proposed. Other lines, e.g., the $1s^2 2s 2p^2\,^4P - 1s2s2p^3\,^4S$ transition expected at 43.235 Å, have not been observed, probably because they are too weak compared to the noise level. Only well-reproducible lines have been taken into account, while those appearing on just one spectrum were probably a noise effect or a deconvolution by-product, and have been ruled out. Table II reports, for each newly determined configuration: the average energy, the Slater parameter values, the composition, and the energy of levels. The Slater parameters, as well as the average energy, are given *ab initio,* as provided by HF calculations, and fitted on the basis of the experimental data through a proper computer code [21], the only exception being the spin-orbit parameter ζ, to which the 95% standard scaling was always applied, inasmuch as no fine structure was observable. Whenever the fit could not be performed, a 90% standard scaling was applied also to the electrostatic "direct" and "exchange" interactions F^k and G^k. Unless differently stated, the composition is to be intended as 100% pure; otherwise this is indicated in its three main LS components, neglecting those below 1%. For completeness, not only are there given the levels corresponding to observed lines, but the whole set of each configuration, including also those with a very low transition probability. Still, there are some unidentified lines left, although a much wider set of configurations was computed than that listed in Table I; however, most of the weaker transitions are missing on our spectra, and some others are expected to appear just beyond our experimental range. Although we claim that a very good selection has been obtained with respect to the other ionization stages, some C I and C III lines have been observed. So, probably, some of the unidentified ones indicated in Table I could also belong to those ions.

The absorption process $1s^2 2s 2p 3p$-$1s2s2p^2 3p$ has also been taken into account. Its analysis turned out to be engaging. On the whole, i.e., including forbidden transitions, there are more than 1000 possible lines for this excitation. They range roughly from 43.6 to 41.3 Å. If we consider only the most probable ones, a good match has actually been found among those belonging to $1s^2 2s 2p(^1P)3p$-$1s2s2p^2 3p$ and some of the observed peaks. However, the strongest transitions for the case ^3P parent should appear around 42.5 Å, whereas nothing was detected there, and, moreover, the $(^1P)3p$ starting terms are not known in literature. Therefore identifications corresponding to this array have been re-

TABLE II. Averaged energies (in cm^{-1}), Slater parameters, and composition of the C II excited levels.

		$1s2s^22p^2$	
E_{av}	2 315 825→	2 315 112	
$F^2(pp)$	74 291	58 794	79%
ζ	115	109	95%
$G^1(sp)$	28 676	29 460	103%
2 298 145		$(^3P)\,^4P_{1/2}$	
2 298 200		$(^3P)\,^4P_{3/2}$	
2 298 291		$(^3P)\,^4P_{5/2}$	
2 322 166		$(^1D)\,^2D_{3/2}$	
2 322 167		$(^1D)\,^2D_{5/2}$	
2 327 622		$(^3P)\,^2P_{1/2}$	
2 327 734		$(^3P)\,^2P_{3/2}$	
2 343 334		$(^1S)\,^2S_{1/2}$	

		$1s2s^22p3p'$	
E_{av}	2 484 643	2 478 790	
ζ	143	136	95%
ζ^{3d} 9.480	0.4 14	13	95%
$F^2(pp')$	11 274	9 840	87%
$G^1(sp)$	35 446	32 284	91%
$G^1(sp')$	3 573	3 235	92%
$G^0(pp')$	6 194	3 695	60%
$G^2(pp')$	5 055	4 500	89%
2 470 205		$(^3P)\,^4D_{1/2}$	
2 470 243		$(^3P)\,^4D_{3/2}$	
2 470 306		$(^3P)\,^4D_{5/2}$	
2 470 395		$(^3P)\,^4D_{7/2}$	
2 471 538		$98\%(^3P)\,^2P_{1/2}$	$2\%(^1P)\,^2P_{1/2}$
2 471 581		$97\%(^3P)2p_{3/2}$	$2\%(^1P)\,^2P_{3/2}$
2 472 274		$99\%(^3P)\,^4S_{1/2}$	
2 474 525		$(^3P)\,^4P_{1/2}$	
2 474 565		$(^3P)\,^4P_{3/2}$	
2 474 625		$(^3P)\,^4P_{5/2}$	
2 477 303		$98\%(^3P)\,^2D_{3/2}$	$2\%(^1P)\,^2D_{3/2}$
2 477 437		$98\%(^3P)\,^2D_{5/2}$	$2\%(^1P)\,^2D_{5/2}$
2 481 167		$95\%(^3P)\,^2S_{1/2}$	$5\%(^1P)\,^2S_{1/2}$
2 494 652		$98\%(^1P)\,^2D_{3/2}$	$2\%(^3P)\,^2D_{3/2}$
2 494 641		$98\%(^1P)\,^2D_{5/2}$	$2\%(^3P)\,^2D_{5/2}$
2 495 718		$98\%(^1P)\,^2P_{1/2}$	$2\%(^3P)\,^2P_{1/2}$
2 495 748		$98\%(^1P)\,^2P_{3/2}$	$2\%(^3P)\,^2P_{3/2}$
2 497 949		$95\%(^1P)\,^2S_{1/2}$	$5\%(^3P)\,^2S_{1/2}$

		$1s2s^22p4p'$	
E_{av}	2 519 514	2 512 649	
ζ	145	138	95 %
ζ'	5	5	95%
$F^2(pp')$	3 767	3 270	87%
$G^1(sp)$	35 786	30 908	86%
$G^1(sp')$	1 324	1 218	92%
$G^0(pp')$	1 995	1 200	60%
$G^2(pp')$	1 725	1 535	89%
2 506 356		$(^3P)\,^4D_{1/2}$	
2 506 392		$(^3P)\,^4D_{3/2}$	
2 506 452		$(^3P)\,^4D_{5/2}$	
2 506 538		$(^3P)\,^4D_{7/2}$	
2 507 116		$61\%(^3P)\,^4S_{3/2}$	$38\%(^3P)\,^2P_{3/2}$
2 507 005		$(^3P)\,^2P_{1/2}$	
2 507 033		$61\%(^3P)\,^2P_{3/2}$	$38\%(^3P)\,^4S_{3/2}$
2 507 776		$(^3P)\,^4P_{1/2}$	
2 507 820		$(^3P)\,^4P_{3/2}$	
2 507 872		$(^3P)\,^4P_{5/2}$	
2 508 867		$(^3P)\,^2D_{3/2}$	
2 508 988		$(^3P)\,^2D_{5/2}$	
2 510 345		$(^3P)\,^2S_{1/2}$	
2 527 934		$(^1P)\,^2D_{3/2}$	
2 527 934		$(^1P)\,^2D_{5/2}$	
2 528 889		$(^1P)\,^2S_{1/2}$	
2 528 250		$(^1P)\,^2P_{1/2}$	
2 528 260		$(^1P)\,^2P_{3/2}$	

		$1s2s^22p5p'$	
E_{av}	2 533 349	2 528 398	
ζ	145	138	95%
ζ'	3	2	95%
$F^2(pp')$	1 709	1 538	90%
$G^1(sp)$	35 886	32 298	90%
$G^1(sp')$	629	566	90%
$G_0(pp')$	896	806	90%
$G^2(pp')$	793	714	90%
2 522 219		$(^3P)\,^4D_{1/2}$	
2 522 255		$(^3P)\,^4D_{3/2}$	
2 522 313		$(^3P)\,^4D_{5/2}$	
2 522 399		$(^3P)\,^4D_{7/2}$	
2 522 609		$92\%(^3P)\,^4S_{3/2}$	$8\%(^3P)\,^2P_{3/2}$
2 522 679		$(^3P)\,^2P_{1/2}$	
2 522 751		$92\%(^3P)\,^2P_{3/2}$	$8\%(^3P)\,^4S_{3/2}$
2 523 400		$(^3P)\,^4P_{1/2}$	
2 523 444		$(^3P)\,^4P_{3/2}$	
2 523 493		$(^3P)\,^4P_{5/2}$	
2 523 780		$(^3P)\,^2D_{3/2}$	
2 523 900		$(^3P)\,^2D_{5/2}$	
2 524 521		$(^3P)\,^2S_{1/2}$	
2 544 390		$(^1P)\,^2D_{3/2}$	
2 544 390		$(^1P)\,^2D_{5/2}$	
2 544 777		$(^1P)\,^2P_{1/2}$	
2 544 781		$(^1P)\,^2P_{3/2}$	
2 544 830		$(^1P)\,^2S_{1/2}$	

		$1s2s^22p6p'$	
E_{av}	2 540 329	2 537 520	
ζ	146	138	95%
ζ'	1	1	95%
$F^2(pp')$	918	826	90%
$G^1(sp)$	35 926	32 334	90%
$G^1(sp')$	346	312	90%
$G^0(pp')$	479	431	90%
$G^2(pp')$	429	386	90%
2 531 652	$98\%(^3P)\,^4D_{1/2}$	$2\%(^3P)\,^2P_{1/2}$	
2 531 687	$99\%(^3P)\,^4D_{3/2}$		
2 531 746	$99\%(^3P)\,^4D_{5/2}$		
2 531 833	$(^3P)\,^4D_{7/2}$		
2 531 895	$85\%(^3P)\,^4S_{3/2}$	$12\%(^3P)\,^2P_{3/2}$	$3\%(^3P)\,^4P_{3/2}$
2 531 938	$98\%(^3P)\,^2P_{1/2}$	$2\%(^3P)\,^4D_{1/2}$	

TABLE II. (*Continued*).

2 532 015	86%$(^3P)^2P_{3/2}$	12%$(^3P)^4S_{3/2}$	1%$(^3P)^2D_{3/2}$
2 532 305	99%$(^3P)^4P_{1/2}$		
2 532 359	96%$(^3P)^4P_{3/2}$	3%$(^3P)^4S_{3/2}$	
2 532 403	98%$(^3P)^4P_{5/2}$	1%$(^3P)^2D_{5/2}$	
2 532 519	99%$(^3P)^2D_{3/2}$	1%$(^3P)^2P_{3/2}$	
2 532 636	98%$(^3P)^2D_{5/2}$	2%$(^3P)^4P_{5/2}$	
2 532 955	99%$(^3P)^2S_{1/2}$		
2 553 598	$(^1P)^2D_{3/2}$		
2 553 598	$(^1P)^2D_{5/2}$		
2 553 801	$(^1P)^2P_{1/2}$		
2 553 805	$(^1P)^2P_{3/2}$		
2 553 831	$(^1P)^2S_{1/2}$		

$1s2s'2p^3$

E_{av}	2 385 529	2 392 481	
$F^2(pp)$	73 275	60 066	82%
ζ	112	106	95%
$G^0(ss')$	18 400	17 919	97%
$G^1(sp)$	27 968	22 420	80%
$G^1(s'p)$	92 192	82 375	89%

2 309 500	$(^3S)(^4S)^6S_{5/2}$		
2 358 579	(52% $^1S)(^4S)^4S_{3/2}$	(48% $^3S)(^4S)^4S_{3/2}$	
2 366 055	$(^3S)(^2D)^4D$		
2 380 471	$(^3S)(^2P)^4P$		
2 401 594	(51% $^1S)(^2D)^2D$	(49% $^3S)(^2D)^2D$	
2 416 009	(51% $^1S)(^2P)^2P$	(49% $^3S)(^2P)^2P$	
2 435 986	(51% $^3S)(^4S)^4S$	(49% $^1S)(^4S)^4S$	
2 436 221	(51% $^3S)(^2D)^2D$	(49% $^1S)(^2D)^2D$	
2 449 224	$(^3S)(^4S)^2S$		
2 450 639	(51% $^3S)(^2P)^2P$	(46% $^1S)(^2P)^2P$	

$1s2s^22p3s'$

E_{av}	2 466 267	2 463 811	
ζ	143	136	95%
$G^1(sp)$	35 427	31 885	90%
$G^0(ss')$	2 455	2 209	90%
$G^1(ps')$	5 494	4 944	90%
2 456 455		$(^3P)^4P_{1/2}$	
2 456 523		$(^3P)^4P_{3/2}$	
2 456 638		$(^3P)^4P_{5/2}$	
2 462 255		$(^3P)^2P_{1/2}$	
2 462 385		$(^3P)^2P_{3/2}$	
2 479 764		$(^1P)^2P_{1/2}$	
2 479 771		$(^1P)^2P_{3/2}$	

$1s2p^4$

E_{av}	2 481 454	2 476 105	
$F^2(pp)$	72 531	66 252	91%
ζ	109	104	95%
$G^1(sp)$	27 415	25 327	92%
2 459 800		$(^3P)^4P_{1/2}$	
2 459 748		$(^3P)^4P_{3/2}$	
2 459 661		$(^3P)^4P_{5/2}$	
2 484 782		$(^1D)^2D_{3/2}$	
2 484 057		$(^1D)^2D_{5/2}$	
2 485 110		$(^3P)^2P_{1/2}$	
2 485 011		$(^3P)^2P_{3/2}$	
2 507 908		$(^1S)^2S_{1/2}$	

$1s2s'2p^23p$

E_{av}	2 547 267	2 541 440	
$F^2(pp)$	81 129	73 016	90%
ζ	134	127	95%
ζ'	14	14	95%
$F^2(p^2p)$	11 461	10 315	90%
$G^0(ss')$	20 591	18 532	90%
$G^1(sp^2)$	33 126	29 814	90%
$G^1(sp)$	3 554	3 199	90%
$G^1(s'p^2)$	97 714	87 943	90%
$G^1(s'p)$	4 052	3 647	90%
$G^0(p^2p)$	5 925	5 333	90%
$G^2(p^2p)$	5 084	4 575	90%

$1s2s^22p3d$

E_{av}	2 499 526	2 499 526	
ζ	145	138	95%
ζ'	1	1	95%
$F^2(pd)$	7 916	7 124	90%
$G^1(sp)$	35 798	32 218	90%
$G^2(sp)$	23	21	90%
$G^1(pd)$	4 416	3 974	90%
$G^3(pd)$	2 506	2 256	90%
2 493 655		$(^3P)^4D_{1/2}$	
2 493 670		$(^3P)^4D_{3/2}$	
2 493 693		$(^3P)^4D_{5/2}$	
2 493 723		$(^3P)^4D_{7/2}$	
2 495 153		$(^3P)^4P_{1/2}$	
2 495 121		$(^3P)^4P_{3/2}$	
2 495 066		$(^3P)^4P_{5/2}$	
2 496 393		$(^3P)^2P_{1/2}$	
2 496 322		$(^3P)^2P_{3/2}$	
2 517 021		$(^1P)^2P_{1/2}$	
2 517 027		$(^1P)^2P_{3/2}$	
2 492 758		$(^3P)^2D_{3/2}$	
2 492 795		$(^3P)^2D_{5/2}$	
2 493 213		$(^3P)^4F_{3/2}$	
2 493 246		$(^3P)^4F_{5/2}$	
2 493 297		$(^3P)^4F_{7/2}$	
2 493 375		$(^3P)^4F_{9/2}$	
2 514 884		$(^1P)^2D_{3/2}$	
2 514 887		$(^1P)^2D_{5/2}$	
2 495 574		$(^3P)^2F_{5/2}$	
2 495 692		$(^3P)^2F_{7/2}$	
2 515 699		$(^1P)^2F_{5/2}$	
2 515 688		$(^1P)^2F_{7/2}$	

garded as being not sufficiently reliable and, consequently, are not given in the table. To some extent, this is also true for the case $1s^22s2p^2$-$1s2s2p^23p$, which is featured by 450 transitions between 40 and 43 Å, with the strongest lines lying around 42 Å. Among these, the two most intense ones could be assigned to observed peaks. Anyway, a more extended attribution is required to confirm these identifications. Because of this, the list of the 77 levels arising from this excited configuration has been omitted and only the energy parameters are shown in the table. Finally, the series $1s^22s^22p$-$1s2s^22pnp$ could be followed up to $n=6$, but for members with parent ^1P no term separation has been detectable beyond $n=4$.

By means of the formula given by Edlén [22], we have tried to deduce the series limits. The values found are 2 549 000 cm^{-1}, i.e., 39.23 Å, for C III $1s2s^22p\ ^3P$ and 2 570 000 cm^{-1}, i.e., 38.91 Å, for C III $1s2s^22p\ ^1P$.

On the basis of the smoothness of the effective quantum number n^* along the series, and taking into account the experimental accuracy, an uncertainty of at least ± 1 kK has been estimated; this error bar is about the same in both cases and corresponds roughly to ± 0.02 Å in that energy region. Looking now at the related C III transitions, these results yield the wavelengths 42.51 Å for $1s^22s^2\ ^1S-1s2s^22p\ ^3P$ and 42.14 Å for $1s^22s^2\ ^1S$-$1s2s^22p\ ^1P$. They are indeed in very good agreement with figures given by Schneider *et al.* [23]. However, it is obvious that such principal quantum numbers do not configure an extended series, as it is instead required in order to be really confident with extrapolation.

CONCLUSION

The *K*-shell absorption spectra of the C isonuclear sequence (C I–C V) have been completed with the present C II spectrum. This absorption spectrum has been obtained with a technique using two laser-produced plasmas. Both the discrete spectrum as well as the photoionization continuum have been observed. Careful wavelength measurements and atomic structure calculations have been performed. The relative photoionization cross section has been measured from the threshold at about 318 eV up to 500 eV and has been compared with independent theoretical result, showing very good agreement. The discrete lines have been identified corresponding to transitions of the 1*s* inner electron starting from the ground and lower-lying excited levels. The main series $1s^22s^22p$-$1s2s^22pnp$ has been measured up to $n=6$. The limits have been estimated at 2 549 000 cm^{-1} (316.0 eV) and 2 570 000 cm^{-1} (318.6 eV) and have been checked against the corresponding C III levels.

ACKNOWLEDGMENTS

The authors wish to thank Professor G. Tondello for many helpful discussions. One of the authors (M. G.) was supported by University of Trento, Italy, through a cooperation program with University of Dakar, Senegal. M. G. is presently with ITNA University C. A. Diop, Dakar, Senegal.

[1] G. Tondello, E. Jannitti, and A. M. Malvezzi, Phys. Rev. A **16**, 1705 (1977).
[2] A. M. Malvezzi, L. Garifo, E. Jannitti, P. Nicolosi, and G. Tondello, J. Phys. B **12**, 1437 (1979).
[3] E. Jannitti, P. Nicolosi, and G. Tondello, Opt. Lett. **4**, 187 (1979).
[4] P. Nicolosi, E. Jannitti, and G. Tondello, Appl. Phys. **B26**, 117 (1981).
[5] P. K. Carroll and E. T. Kennedy, Phys. Rev. Lett. **38**, 1068 (1977).
[6] E. Jannitti, M. Mazzoni, P. Nicolosi, G. Tondello, and W. Yongchang, J. Opt. Soc. Am. B **2**, 1078 (1985).
[7] E. Jannitti, F. Pinzhong, and G. Tondello, Phys. Scr. **33**, 434 (1986).
[8] E. Jannitti, P. Nicolosi, and G. Tondello, Phys. Scr. **36**, 93 (1987).
[9] E. Jannitti, P. Nicolosi, G. Tondello, Z. Yongzhen, and M. Mazzoni, Opt. Commun. **63**, 37 (1987).
[10] E. Jannitti, P. Nicolosi, and G. Tondello, Phys. Lett. A **131**, 186 (1988).
[11] E. Jannitti, P. Nicolosi, and G. Tondello, in *X-Ray and VUV Interaction Data Bases, Calculations and Measurements,* edited by N. K. Del Grande, Proc. SPIE **911**, 11 (1988).
[12] F. E. Irons, R. W. P. McWhirter, and N. J. Peacock, J. Phys. B **5**, 1975 (1972).
[13] E. Jannitti, P.Nicolosi, and G. Tondello, Phys. Scr. **41**, 458 (1990).
[14] R. F. Reilman and S. T. Manson, Astrophys. J. Suppl. Ser. **40**, 815 (1979).
[15] E. Jannitti, P. Nicolosi, and G. Tondello, in *X-Ray and VUV Interaction Data Bases, Calculations and Measurements* (Ref. [11]), p. 157.
[16] P. A. Jansson, *Deconvolution with Applications in Spectroscopy* (Academic, New York, 1984).
[17] M. Mazzoni and P. Nicolosi (unpublished).
[18] M. Rødbro, R. Bruch, and P. Bisgaard, J. Phys. B **12**, 2413 (1979).
[19] R. D. Cowan, *The Theory of Atomic Structure and Spectra* (University of California Press, Berkeley, 1981).
[20] C. E. Moore, *Atomic Energy Levels,* Natl. Bur. Stand. (U.S.) Circ. No. 467 (U.S. GPO, Washington, DC, 1949), Vol. 1.
[21] G. E. Bromage, The Cowan Zealot Suite, Science Research Council, Appleton Laboratory, Culham, U. K., 1978 (unpublished).
[22] B. Edlén, in *Spectroscopy I,* edited by S. Flugge, Handbuch der Physik Vol. 27 (Springer-Verlag, Berlin, 1964), p. 154.
[23] D. Schneider, R. Bruch, W. H. E. Schwarz, and T. C. Chang, Phys. Rev. A **15**, 926 (1977).